Integrated Design and Multi-objective Optimization of a Single Stage Heat-Pump Turbocompressor

J. Schiffmann
Laboratory for Applied Mechanical Design,
Ecole Polytechnique Fédérale de Lausanne,
Neuchâtel 2000, Switzerland
e-mail: jurg.schiffmann@epfl.ch

Small-scale turbomachines in domestic heat pumps reach high efficiency and provide oil-free solutions, which improve heat-exchanger performance and offer major advantages in the design of advanced thermodynamic cycles. An appropriate turbocompressor for domestic air based heat pumps requires the ability to operate on a wide range of inlet pressure, pressure ratios, and mass flows, confronting the designer with the necessity to compromise between range and efficiency. Further, the design of small-scale direct driven turbomachines is a complex and interdisciplinary task. Textbook design procedures propose to split such systems into subcomponents and to design and optimize each element individually. This common procedure, however, tends to neglect the interactions between the different components leading to suboptimal solutions. The author proposes an approach based on the integrated philosophy for designing and optimizing gas bearing supported, direct driven turbocompressors for applications with challenging requirements with regards to operation range and efficiency. Using experimentally validated reduced order models for the different components an integrated model of the compressor is implemented and the optimum system found via multi-objective optimization. It is shown that compared to standard design procedures, the integrated approach yields an increase of the seasonal compressor efficiency of more than 12 points. Further, a design optimization based sensitivity analysis allows to investigate the influence of design constraints determined prior to optimization such as impeller surface roughness, rotor material, and impeller force. A relaxation of these constrains yields additional room for improvement. Reduced impeller force improves efficiency due to a smaller thrust bearing mainly, whereas a lighter rotor material improves rotordynamic performance. A hydraulically smoother impeller surface improves the overall efficiency considerably by reducing aerodynamic losses. A combination of the relaxation of the three design constraints yields an additional improvement of six points compared to the original optimization process. The integrated design and optimization procedure implemented in the case of a complex design problem thus clearly shows its advantages compared to traditional design methods by allowing a truly exhaustive search for optimum solutions throughout the complete design space. It can be used for both design optimization and for design analysis. [DOI: 10.1115/1.4029123]

Introduction

In turbomachinery, a trend toward downscaling and increased rotor speeds has become evident over the last decade [1]. Small-scale turbomachinery is of particular interest due to the high power density compared to other technology. Recent experimental investigations in domestic heat-pump compressor systems demonstrate the potential of turbocompressors to increase power density compared to equivalent volumetric machines. In addition, they reach high efficiency and provide oil-free solutions, which improve heat-exchanger performance and offer major advantages in the design of advanced thermodynamic cycles [2]. An appropriate turbocompressor for domestic air based heat pumps requires the ability to operate on a wide range of inlet pressures, pressure ratios, and mass flows, confronting the designer with the necessity to search for a compromise between range and efficiency [3]. Table 1 represents the typical specification for the first stage compressor of a twin stage air–water heat-pump cycle with an open economizer delivering a heat rate of 12 kW at a water temperature of 60 °C with an air temperature of −12 °C using R134a as a refrigerant fluid. A typical radial compressor tip diameter for these specifications is around 20 mm requiring rotational speeds in excess of 200 krpm. The combination of high efficiency, hermetic design, high rotor speeds, and the requirement for maintenance free operation over a duration of 20 years calls for dynamic gas

Table 1 Heat-pump compressor specifications for the first stage of a twin stage air–water heat pump delivering a heat rate of 12 kW at −12 °C external air temperature [3]

OP	A-12	A-7	A2	A7	A12
T_{Air} (°C)	−12	−7	2	7	12
T_{Water} (°C)	60	55	50	45	40
p_{in} (MPa)	0.144	0.177	0.251	0.302	0.36
Π	4.17	3.39	2.39	1.99	1.67
m (kg s^{-1})	0.053	0.043	0.024	0.016	0.005

Contributed by the Heat Transfer Division of ASME for publication in the Journal of Turbomachinery. Manuscript received September 9, 2013; final manuscript received October 25, 2014; published online December 23, 2014. Assoc. Editor: Stephen W. T. Spence.

bearings, which are lubricated directly with the processed refrigerant fluid.

Nature of the Issues. A direct driven turbocompressor can be divided into three subcomponents: (1) the electric motor, (2) the impeller(s), and (3) the spindle unit, which is composed of rotor and bearings and which carries both the impeller(s) and the rotor of the electric motor. Although the main components have well defined tasks they interact with each other in different, often complex ways. In addition, the design of such an intricate system involves many engineering disciplines thus calling for truly interdisciplinary design approaches.

According to standard design procedures as proposed by VDI [4], or by Pahl et al. [5], the way in dealing with complex interdisciplinary system design is functional decomposition. The system to be designed is split into several subcomponents according to the modular nature and/or to the disciplines involved. However, in order to make such a procedure work adequately, it is necessary to fix key design parameters at a very early stage in the design process such that component specifications may be defined and the individual element design and optimization delegated to different specialist groups. The determination of early stage design parameters is generally based on experience of previous designs and exposes standard design procedures to several pitfalls: (1) the key parameters fundamentally define the overall system design, thus not only restricting the solution space but also potentially limiting maximum achievable performance, (2) the procedure is suggested to guide the design process toward conventional, already existing and proven designs, hence decreasing the incentive to explore alternative solutions, and (3) once the primary design is fixed, each component is optimized individually. That means that the interactions between the different elements are likely to be neglected during the subsequent design stages.

It seems therefore of primary importance to apply integrated design strategies from the kick-off throughout the complete design procedure in order to truly improve the system design process. Maximizing the information flux between the different components from the conceptual to the detailed design stage, and allowing the process to seek for solutions on less common pathways is suggested to yield more efficient design procedures with regards to their outcome.

The issues related to the fragmented component view have been addressed by Jarrett et al. [6] in the domain of jet engines. By linking aerothermal codes with mechanical models, an existing multistage axial compressor design was optimized. The new solution resulted in improved rotor blade creep life, showing that automated and integrated design methods yield the potential for considerable improvement compared to procedures with fragmented component view.

Goals and Objectives. The goal of the investigation is an integrated design and optimization tool for small-scale, gas bearing supported turbocompressors that allows to avoid the pitfalls characteristic to fragmented design procedures. The objectives are: (1) to implement a comprehensive model for gas bearing supported rotors, (2) to implement a model for radial compressors, (3) to link the subcomponents to form a virtual system model, and (4) to connect the system model to a multi-objective optimizer to investigate the effect of an integrated design philosophy approach on system performance compared to the standard fragmented design procedure.

Scope of the Paper. The approach is based on the design process of a turbocompressor for driving domestic heat pumps based on the specifications in Table 1. The radial compressor model used in this investigation is based on work by Schiffmann and Favrat [3], where an experimentally validated tool is presented together with an optimization methodology addressing the design of radial compressors with challenging operating conditions.

The bearings are key components of small-scale turbomachinery, since they need to operate at high rotor speeds. Dynamic gas bearings offer significant advantages over more conventional technology such as improved reliability and decreased maintenance. In addition, they provide an oil-free solution characterized by low mechanical losses. Cross-coupled behavior and limited damping resulting from the low viscosity of gas are, however, main disadvantages. Hence, the prediction of rotordynamic performance is a key step to design stable gas bearing supported rotor. The model for rotors supported on herringbone grooved journal (HGJB) and spiral groove thrust bearings (SGTBs) in this article is based on experimentally validated work by Schiffmann and Favrat [2,7].

The combined rotor and impeller models are able to predict the compressor map, for a given impeller geometry and to characterize the rotordynamic stability of the gas bearing supported rotor directly driving the impeller through an electric motor. The integrated compressor model is linked to a multi-objective optimizer with the objectives to maximize both seasonal performance and rotordynamic stability. The obtained Pareto curve is compared to the design resulting from a classical fragmented approach where each component is optimized individually for maximum performance, thus investigating and demonstrating the advantages of an integrated approach. Further, the new tool is used to perform a sensitivity analysis to investigate the effect on system performance of design constraints such as impeller surface roughness (manufacturing finish), rotor material weight, and measures for reduced axial load.

Integrated Model Description

Axial and Journal Bearing Model. Out of many different topologies, journal and thrust bearings with viscous pumping grooves have been used in this particular application. A reliable model is required to predict the dynamic bearing stiffness and damping coefficients as a function of geometry and operating conditions. Table 2 summarizes the design variables of HGJB and of inward pumping SGTB.

Expressions for groove width, length, and depth ratios are given as follows:

$$H = \frac{h_g + C}{C}, \qquad \alpha = \frac{w_g}{w_g + w_r}, \qquad \gamma = \frac{L_J - L_{Land}}{L_J} \tag{1}$$

Figure 1 illustrates the typical layout of HGJB bearing in an isometric, unwrapped, and cut view. Figure 2 represents a schematic view of an inward pumping SGTB. The shadowed surfaces represent the pumping grooves shaped by logarithmic spirals.

The evolution of the fluid film pressure within the bearing clearance, and therefore bearing properties (stiffness and damping matrices), is governed by the Reynolds equation [8]. The difficulty

Table 2 HGJB bearing and SGTB design parameters

Journal bearing	D_J	Journal diameter
	L_J/D_J	Length to diameter ratio
	C_J	Nominal clearance
	H_J	Groove depth ratio
	α_J	Groove width ratio
	β_J	Groove angle
	γ	Groove length ratio
Thrust bearing	R_0	Outer radius
	R_I	Inner radius
	R_g	Groove inner radius
	C_{Ax}	Nominal clearance
	H_{Ax}	Groove depth ratio
	α_{Ax}	Groove width ratio
	β_{Ax}	Groove angle

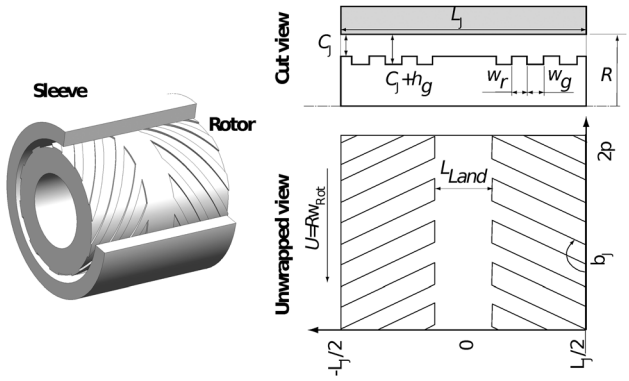

Fig. 1 HGJB layout and nomenclature

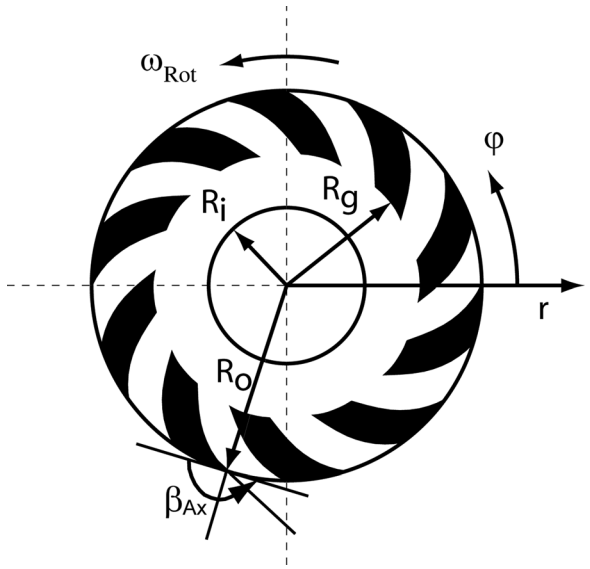

Fig. 2 Inward pumping SGTB layout and nomenclature

in modeling bearings with grooved surfaces is the capturing of the aerodynamic effect of the grooves. The procedure implemented for modeling grooved bearings in this work is based on the narrow groove theory (NGT). The NGT assumes a periodic saw-toothed pressure pattern in the circumferential direction where each pressure rise and fall pair is generated by a groove–ridge pair. Assuming an infinite number of grooves, the saw-toothed pressure approaches a smooth evolution and a modified Reynolds equation is obtained that takes into account for the groove geometry [9]. The nonlinear differential equation is solved by assuming a separation of variables and by applying a perturbation method. Small radial perturbations of the concentric bearing are introduced to yield linearized partial differential equations for the zeroth and first order pressure perturbations. These are obtained by numerical integration and allow to determine the journal and thrust bearing direct and cross-coupled stiffness and damping coefficients. Note that while the static force coefficients depend primarily on rotor speed, the dynamic bearing coefficients such as stiffness and damping are governed by both the zeroth order pressure distribution and the excitation frequency which might be different from the rotor frequency.

The implemented bearing model further includes additional phenomena like clearance distortion resulting from centrifugal forces as described in detail by Schiffmann and Favrat [7]. Real gas and rarefaction effects which may become significant depending on operating conditions and lubricant fluid are taken into account as well [10,11].

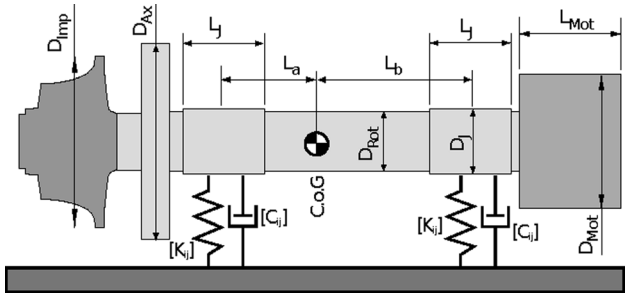

Fig. 3 Rotordynamic model for a rigid-body rotor with overhung motor supported on two journal bearings characterized by their stiffness and damping matrices [*K*] and [*C*]

Rotordynamics. A characteristic feature of gas lubricated bearings is that their properties are not only a function of rotor speed but also depend on excitation frequency. This needs to be taken into account in the rotordynamic stability assessment. The approach here is based on Pan's spectral analysis method [12] extended by Schiffmann and Favrat [2,7]. The rigid-body rotordynamic system is represented in Fig. 3 and described by

$$[M]\ddot{\mathbf{q}} + [B]\dot{\mathbf{q}} + [K]\mathbf{q} = \mathbf{f} \tag{2}$$

where $[M]$ is the system inertia and $[K]$ the bearing stiffness coefficients. $[B]$ is composed of the bearing damping coefficients $[C]$ and gyroscopic effects $[G]$. In this particular case, the motion vector is composed of five degrees of freedom that includes translational displacement in radial and axial direction as well as two tilting motions around the center of gravity. The rotor properties are described in terms of mass M_{Rot}, polar and transverse rotor inertia I_{P}, and I_{T} and location of the bearing midplanes relative to the rotor center of gravity L_{a}, L_{b}. Equation (2) yields an eigenvalue problem with eigenvalues

$$s_j = \lambda_j + i\Omega_j\omega_{\mathrm{Rot}} \tag{3}$$

where the imaginary part $\omega_j = \Omega_j\omega_{\mathrm{rot}}$ represents the damped natural frequency of the whirl motion and λ_j the corresponding damping coefficient. It is common practice to measure rotor stability using the logarithmic decrement defined as

$$\Gamma_j = -\lambda_j \frac{2\pi}{\Omega_j\omega_{\mathrm{Rot}}} \tag{4}$$

Stable operation requires $\Gamma > 0$. To predict the whirl speed and the corresponding stability map of a gas bearing supported rotor, the system is excited over a range of frequencies $\omega_{\mathrm{Ex}} = \Omega\omega_{\mathrm{Rot}}$ while keeping the rotor speed ω_{Rot} constant. A natural whirl frequency is determined when the estimated frequency coincides with the excitation frequency $\Omega_j\omega_{\mathrm{Rot}}$. This procedure is carried out for Ω ranging from 0 up to 3. Pan shows that for higher whirl ratios the bearing properties reach asymptotic values [13]. The rigid-body rotordynamic model estimates the whirl speed and the stability map for a given bearing geometry and a specific rotor configuration (M_{Rot}, I_{T}, I_{P}, L_{a}, L_{b}). The implemented rotor-bearing system can be associated to a mathematical function given as follows:

$$[\Gamma_{\mathrm{Rad}}, \Gamma_{\mathrm{Ax}}] = f_{\mathrm{Rot}}(\mathbf{G}_{\mathrm{J}}, \mathbf{G}_{\mathrm{Ax}}, \mathbf{G}_{\mathrm{Rot}}) \tag{5}$$

where $\mathbf{G}_{\mathrm{J}}$, $\mathbf{G}_{\mathrm{Ax}}$, and $\mathbf{G}_{\mathrm{Rot}}$ stand for the variable vectors characterizing journals, thrust bearing, and rotor geometry.

Different rotor layouts are possible for direct driven turbocompressors. Schiffmann and Favrat [7] have investigated a more classical design with the motor between the journals and compared it to a layout with both motor and impeller overhung.

Optimization results suggest that both designs perform similarly with regards to rotordynamic performance and mechanical losses. The main advantage of the overhung design, however, is easier manufacturing and assembly. The current work therefore focuses on the rotor layout based on the overhung design. Figure 3 shows a schematic representation of the investigated rotor layout and indicates the main rotor dimensions such as journal length (L_J), thrust bearing OD (D_{Ax}), and the distance between the journals and the center of gravity (L_a and L_b), rotor diameter (D_{Rot}), impeller tip diameter (D_{IMP}), and electric motor diameter and length (D_{Mot} and L_{Mot}).

Mechanical Rotor Losses. Rotor and bearing windage losses are not only required for calculating the system performance but also for predicting the bearing thermal clearance distortion resulting from temperature gradients. Only very few experimental data has been published on power losses for gas lubricated bearings. Cunningham et al. [14] investigated load capacity and losses of several HGJB configurations. Rotor and bearing windage losses are based on validated work by Mack [15]. The total mechanical losses are expressed as the sum of the windage losses generated in the bearings, on the rotor and within the rotor–stator gap of the electric motor

$$\dot{E}_{Tot} = \dot{E}_J + \dot{E}_{Ax} + \dot{E}_{Rot} + \dot{E}_{Mot} \tag{6}$$

Impeller. The flow within a radial compressor stage is governed by secondary flows and therefore highly three-dimensional. Accurate flow and performance prediction therefore requires advanced numerical tools. Due to elevated computation time required for predicting accurate flow patterns, reduced order models are often used for designing turbomachinery. Well, calibrated and experimentally validated tools are very rapid and are successfully being applied throughout industry [16]. The reduced order 1D impeller model used in this article is based on velocity triangles and cross-sectional areas defined at the inlet and at the exhaust of each compressor stage section (inducer, impeller, diffuser, and volute). Proven correlations based on the Galvas [17] loss collection allow to include aerodynamic losses such as incidence, skin friction, blade loading, diffusion, tip leakage, and recirculation. Figure 4 represents the layout and design variables of a typical radial compressor stage. Slightly less efficient vaneless diffusers instead of vaned diffusers are used in this work for their larger mass-flow range.

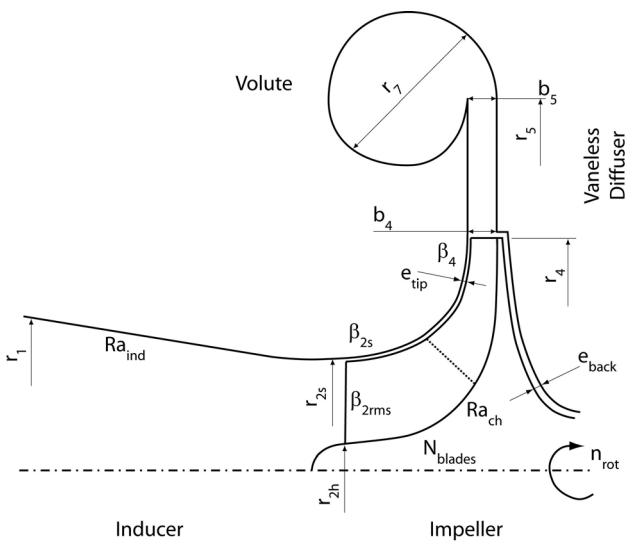

Fig. 4 Radial compressor stage and design variables

The implemented impeller model predicts the compressor map as a function of the impeller stage geometry and operating conditions, i.e., thermodynamic inlet state, rotational speed, and mass flow. Surge prediction is based on the correlations by Senoo and Kinoshita [18]. The mathematical model function is expressed as follows:

$$[\Pi, \eta, \text{surge}, \text{choke}] = f_{Imp}(\mathbf{G}_{Imp}, \omega_{Rot}, \dot{m}, p_{In}, T_{In}) \tag{7}$$

Electric Motor. For this particular application a synchronous, permanent magnet machine has been selected due to its power density and advantages with regards to thermal management and rotordynamic aspects. The motor sizing is based on empirical relations based on the output equation [19] given as follows:

$$\dot{E}_{Mot} = 2\pi R_{Mot}^2 L_{Mot} \tau \omega_{Rot} \tag{8}$$

where R_{mot} and L_{mot} are the diameter and the length of the rotor, respectively, and τ the airgap shear stress.

Surface mounted permanent magnets require a retaining sleeve to prevent them from moving while rotating in order to avoid mass center displacement and shifting unbalance. These sleeves are in general highly stressed and the materials available for these applications are not many. Schiffmann et al. [20] have investigated the possibility of sleeves made of high performance nickel alloys or of carbon fibers composites. The inconvenience of nickel alloys is the high level of preload reaching 95% of the yield stress. Carbon fiber sleeves are more complicated to manufacture and assemble. Binder et al. [21] have compared surface mounted and buried permanent magnet geometries. Surface mounted magnets fixed by a carbon–fiber sleeve are suggested to be the better choice, as considerably higher mechanical strength may be reached, allowing for higher tip speeds. It can be shown that the maximum tip speed for a typical permanent magnet rotor is around 250 ms^{-1} for carbon fiber sleeves.

In terms of rotordynamics, it is desirable that the rotor is as short as possible, i.e., as large as possible in diameter. Using a fixed maximum tip speed for a given rotational speed and required motor power, Eq. (8) allows to calculate the required rotor length. The proposed procedure does not include any electrical design, of course. Note that in terms of windage losses the motor should be as slim as possible. Hence, a compromise between rotordynamic performance and efficiency is required.

System Model. In order to build an integrated system model, the different components have been linked together to form an overall mathematical function that allows to predict the performance of the complete compressor system as a function of system geometry and operating conditions. The mathematical expression of the integrated system model is given as follows:

$$[\eta_{Sys}, \Gamma_{Rad/Ax}] = f_{Sys}(\mathbf{G}_J, \mathbf{G}_T, \mathbf{G}_{Rot}, \mathbf{G}_{Mot}, \mathbf{G}_{Imp}, \text{OP}) \tag{9}$$

where $\mathbf{G}_i$ represent the sets of geometry variables defining the design of the different components. Operation point (OP) stands for a set of required heat-pump operating conditions. The seasonal system efficiency η_{Sys} corresponds to an isentropic energy consumption efficiency based on the seasonal energy consumption given as follows:

$$\eta_{Sys} = \frac{\sum \dot{E}_{IS-K}(T_{Ext}) n_d(T_{Ext})}{\sum \frac{\dot{E}_{IS-K}(T_{Ext})}{\eta(T_{Ext})} n_d(T_{Ext})} \tag{10}$$

where n_d represents the occurrence of days at given external air temperatures. The following optimizations are based on the local climate profile of Zürich.

The system function (Eq. (9)) first calculates the compressor map for a given impeller design ($\mathbf{G}_{\mathrm{Imp}}$) to identify whether a particular aerodynamic design is capable of achieving the required OPs. In the case of a mismatch between compressor map and OPs (operation in surged or choked conditions), a zero efficiency and an unstable rotordynamic performance are imposed on the function values and the calculation aborted. If an aerodynamic matching is found, efficiency, impeller thrust forces, and rotor speeds for each OP are predicted in a second step. Together with the bearing geometry ($\mathbf{G}_{\mathrm{J}}$ and $\mathbf{G}_{\mathrm{T}}$), the knowledge of the rotor speeds allows to calculate the mechanical losses and to check whether the thrust bearing yields sufficient load capacity to support the impeller thrust forces. In order to gain time, the calculation is aborted if insufficient load capacity is achieved. In a third step, mechanical power for driving both the impeller and the rotor at the required rotor speeds is used to size the electric motor (Eq. (8)). This step is an iterative one, since the motor windage losses depend on its geometry. The size of the impeller and the motor allows to predict weight, inertias, and the position of the center of gravity of the complete rotor prior to the rotordynamic calculations, which ultimately yield radial and axial stability margins (Γ_{Rad} & Γ_{Ax}) in a fourth step.

Model Limitations. The stiffness and damping coefficients obtained by the bearing model are not suitable for estimating large orbits resulting from a significant unbalance, since the approach is based on small perturbations around a concentric rotor position. The model, however, is adequate to perform a conservative rotordynamic stability analysis and has been validated experimentally [22].

The impeller design is based on a reduced order model. The highly three-dimensional flow pattern in the radial compressor is modeled via a one-dimensional analysis coupled to empirical loss correlations. Hence, only limited flow physics is captured within the model. Further, as the model is based on inlet and exhaust surfaces and flow angles, it cannot be used to define the detailed evolution of the impeller shroud and hub contours and local blade angles between inlet and exhaust. More advanced design tools are required to complete this step. Experimental investigations at similar scale presented in previous work, however, show good agreement between model and measurements [3].

The design of the electric motor is based on an electromagnetic output formulation, which does not include any detailed electric and thermal design. The used equation, however, is accurate enough to predict the rotor size as a function of the required mechanical power.

Integrated Design and Optimization

The optimization objective is to maximize both the seasonal system efficiency and rotordynamic stability and is mathematically expressed as follows:

$$\begin{bmatrix} \max(\eta_{\mathrm{Sys}}) \\ \max(\Gamma_{\mathrm{Rad/Ax}}) \end{bmatrix} = f_{\mathrm{Sys}}(\mathbf{G}_{\mathrm{J}}, \mathbf{G}_{\mathrm{T}}, \mathbf{G}_{\mathrm{Rot}}, \mathbf{G}_{\mathrm{Mot}}, \mathbf{G}_{\mathrm{Imp}}, \mathrm{OP}) \tag{11}$$

and is subject to the following constraints:

$$\begin{aligned} & C_{\mathrm{J}} \geq 2\ \mu\mathrm{m} \\ & K_{\mathrm{Eq}} \cdot C_{\mathrm{J}} \cdot 0.8 \geq \max(F_{\mathrm{A}}, F_{\mathrm{B}}) | \omega_{\mathrm{Rot}} = 0.05 \cdot \omega_{\mathrm{Max}} \\ & F_{\mathrm{Imp}} \leq F_{\mathrm{Ax}}(\varepsilon = 0.7) \\ & \omega_{\mathrm{Bend}} \geq 1.2 \cdot \omega_{\mathrm{Rot}} \\ & \text{surge and choke} = 0 \end{aligned} \tag{12}$$

which ensure that the journal bearing clearance remains larger than 2 μm on the complete operating range and that the journal bearings yield sufficient load capacity to carry the rotor at low rotor speed. Further, the thrust bearing is required to support the impeller axial load at a maximum relative eccentricity of 70%. In addition, the first critical rotor bending frequency needs to be larger than the maximum rotational speed (20%), and the compressor is not supposed to operate in surged or choked conditions.

The objectives of maximizing both the seasonal efficiency and the rotordynamic performance are of conflicting nature. Hence, this optimization procedure attempts to find the ideal trade-off between the two conflicting objectives, which is represented by the Pareto frontier. The traditional approach for such problems consists in combining the different objectives with weighting factors into a single design criterion. This procedure calls for several optimizations runs to perform a sensitivity analysis on the weighting factors to justify a choice of weights. This methodology is therefore impractical and exceedingly time-consuming. In contrast to the objective weighting procedure, true multi-objective optimization keeps the objectives as equal entities and provides detailed and distortion-free information about the ideal trade-off to the decision making engineer.

The multi-objective optimization process in this paper is performed by coupling the integrated system model (Eq. (9)) to a clustering Pareto evolutionary algorithm [23], which has been successfully used in similar optimization problems [7,24]. Prior work on this algorithm was motivated by the requirement of a true multi-objective optimization tool that may be applied on a wide range of optimization problems without the need of tuning, while producing a homogeneous distribution along the Pareto frontier [23]. The optimization tool is based on genetic algorithms and is started with a randomly selected initial population of solutions. New generations are created out of the existing population by variable crossover and mutation. The new population is ranked and thinned to avoid too large numbers of solutions and to keep up convergence pressure. The removal of individual solutions is performed based on their ranking, while keeping descendants in the tail areas to maintain diversity. The optimization tool tunes both crossover and mutation automatically to improve convergence and to achieve a uniform distribution on the resulting frontier. Further in-depth detail about the multi-objective optimizer tool can be found in work by Leyland [25].

The current optimization process is initialized with a starting population of 1000 randomly selected solutions and stopped after achieving satisfactory convergence, which corresponds to approximately 50,000 evaluations in this application. Convergence is tested on both the Pareto frontier and the relative motion of the design variables between parents and descendants. The computation was performed on a computer cluster of 20 nodes and took approximately 12 h.

The design variables and their ranges used for the optimization are summarized in Table 3. Note that both the outer diameter of thrust disk and motor are normalized with regards to a threshold value. The limits are imposed by structural considerations resulting from centrifugal stress. For the thrust disk and for the rotor of the electric motor, the limit speed is 340 ms^{-1} and 240 ms^{-1}, respectively.

Prior to the integrated optimization, the small-scale proof of concept compressor system was designed by applying a fragmented design and optimization procedure. Each component was optimized individually for minimal losses and maximum rotordynamic stability. The same multi-objective optimization tool was used and the same design variables applied as for the integrated approach. The first prototype design was used to prove the feasibility of small-scale, oil-free turbocompressors and to both calibrate and validate the models which are used in this work.

The Pareto curve resulting from the integrated optimization is represented in Fig. 5 where it is compared to the performance of the fragmented component view design. Compared to the proof of concept, the integrated approach improves the system performance by 12 points for the same logarithmic decrement, thus validating the proposed design methodology, which is based on experimentally validated reduced order models. It is suggested

Table 3 System geometry variables for the optimization

		Range
Journal bearing	D_J	5–15 mm
	L_J/D_J	1–2
	C_J	2–10 μm
	H_J	0–5
	α_J	0.4–0.6
	β_J	110–170 deg
	γ	0.1–1
Rotor	D_{Rot}/D_J	0.5–1
	l_1	5–25 mm
	D_{Mot}/D_{Max}	0.5–1
	Material	Type A
Thrust bearing	$R_0/R_{0\ Max}$	0.5–1
	R_I	$D_J/2$
	$(R_0 - R_g)/(R_0 - R_i)$	0.1–0.9
	C_{Ax}	5–20 μm
	H_{Ax}	0–5
	α_{Ax}	0.4–0.6
	β_{Ax}	110–170 deg
Impeller	r_{2s}/r_{2h}	0.2–0.4
	r_{2s}/r_4	0.15–0.8
	R_4	2–35 mm
	b_4/r_4	0.0015–0.3
	N_{Bl}	5–11
	β_4	−45–0 deg
Dependent parameters	R_1	$1.1 \cdot r_{2s}$
	L_{Ind}	$4 \cdot r_4$
	R_5	$1.5 \cdot r_4$
	e_{tip}	$0.2 \cdot r_4^2$
	e_{back}	$0.04 \cdot r_4$
	N_{Sp}	B_4
	β_5	N_{Bl}
	e_{blade}	0.2 mm
	Ra_{Ind}	1.2×10^{-5} mm
	Ra_{Imp}	1.2×10^{-5} mm

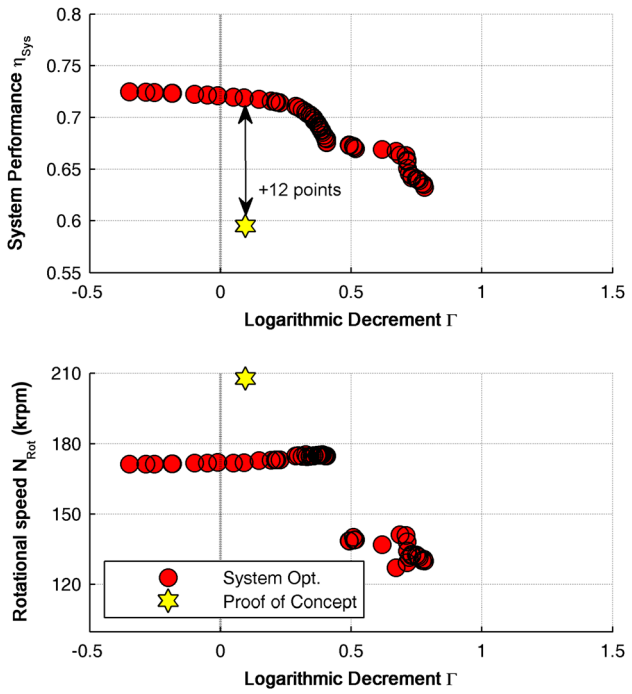

Fig. 5 Evolution of Pareto optimum system performance and rotational speed required to reach OP A-7 as function of rotordynamic stability

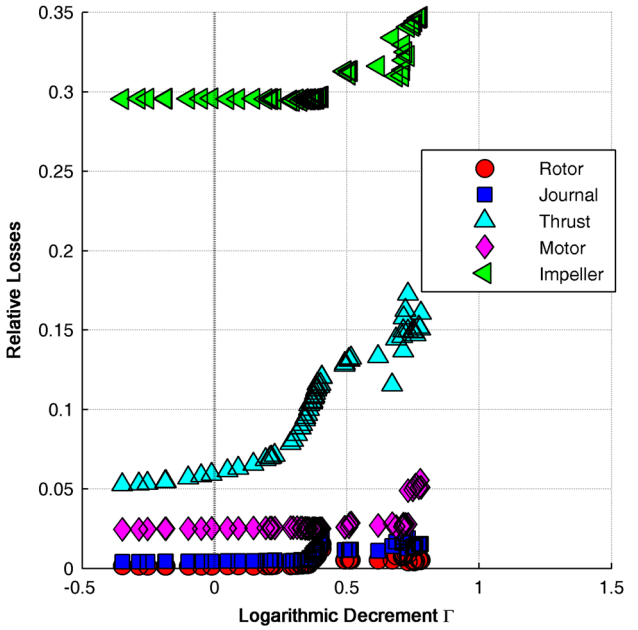

Fig. 6 Evolution of cumulated seasonal losses associated to aerodynamic and windage losses generated by impeller, bearings, rotor, and motor

that the underlying mechanism resulting in the proof-of-concept design falling off the Pareto front is the disregard for mutual component interactions by applying a fragmented component approach.

The second inset of Fig. 5 shows the Pareto optimum rotational speed required to reach OP A-7. The integrated approach results in lower rotational speeds compared to the fragmented design. The evolution of aerodynamic losses versus specific speed, however, suggests that efficiency drops considerably quicker at reduced rotor speeds compared to increased speeds. At high rotor speeds, the losses are dominated by high relative flow velocities within the impeller, while disk friction and leakage dominate the losses at low rotor speeds [26]. This rotor speed reduction resulting from the integrated approach therefore suggests that mechanical losses incurred by motor, rotor, and gas lubricated bearings as well as rotordynamic considerations tend to push the small-scale compressors speed toward lower values than expected by traditional scaling laws established for machines operating at large scale [26,27].

Figure 6 shows how the cumulated relative seasonal losses evolve along the Pareto curve as a function of rotordynamic stability. Together with Fig. 5, the results allow the following conclusions: (1) the integrated approach tends toward increased impeller tip diameter to reduce rotational speed which mitigates windage losses especially of the electric motor, (2) rotordynamic stability is achieved by increased rotor and bearing diameters (increased losses), and (3) the spindle design has a significant impact on overall system performance, hence on design. Neglecting component interactions certainly facilitates the design process but is clearly suggested to yield suboptimum performance.

Sensitivity Analysis

Note that the initial integrated design optimization is based on some preliminary design choices such as rotor material, impeller surface finish, and sealing (thrust force pattern). In order to investigate the influence of these preliminary choices on overall performance, additional optimization runs have been performed where the design variables and ranges are the same as in Table 3 except for the relaxation of the following constraints:

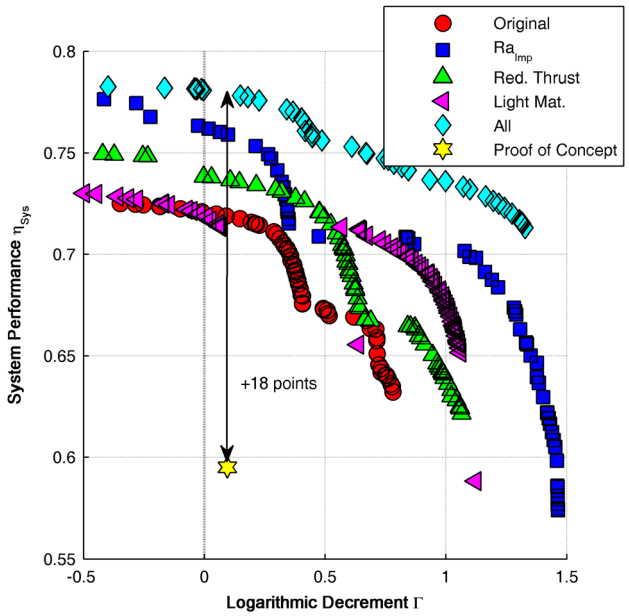

Fig. 7 Evolution of Pareto optimum system performance for relaxed optimization constraints

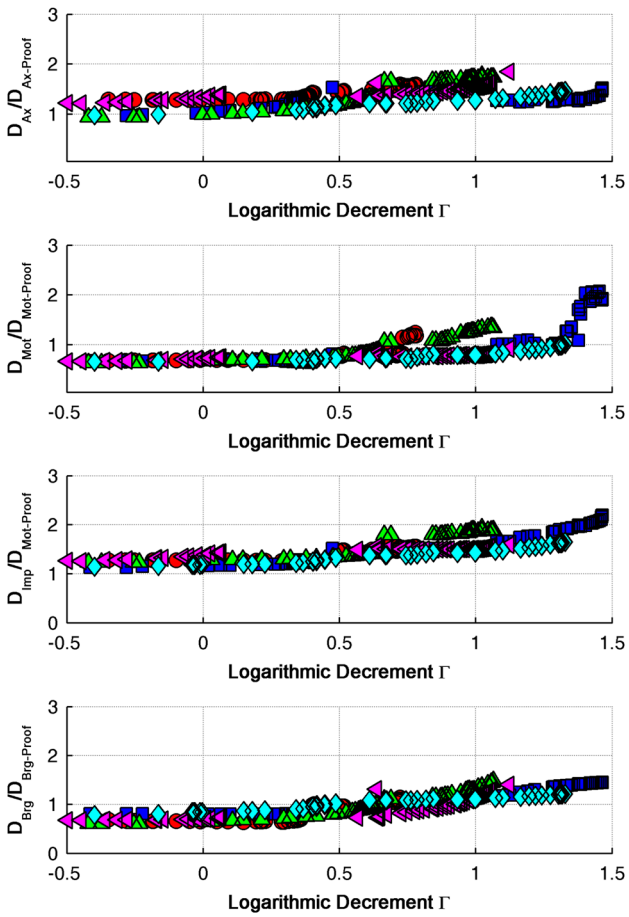

Fig. 8 Evolution of Pareto optimum diameters relative to the proof of concept design

Case 1: impeller thrust force reduced by 50% through appropriate face sealing.
Case 2: use of lighter rotor material, with a density reduced by a factor 4.6 compared to the original optimization.

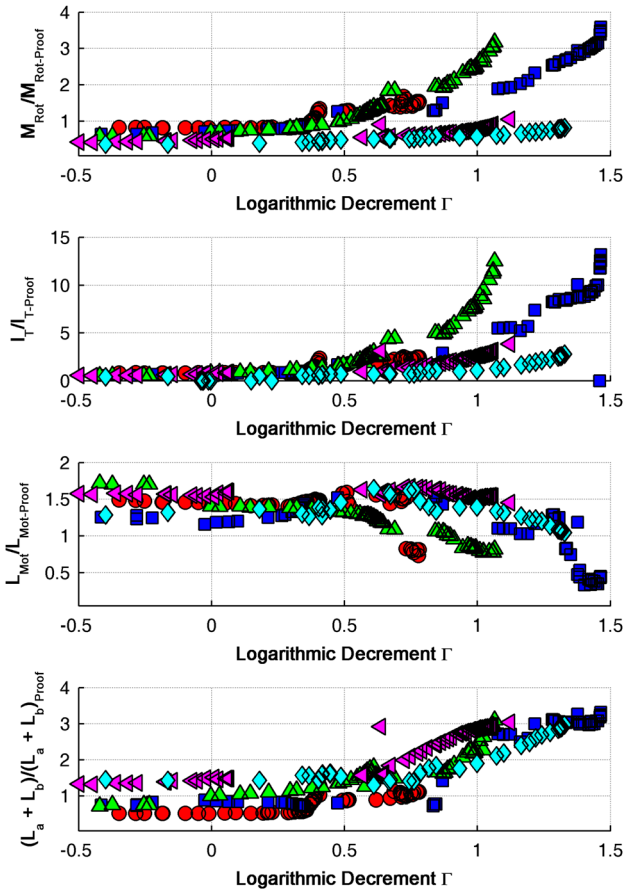

Fig. 9 Evolution of Pareto optimum rotor dimensions relative the proof of concept design as function of stability

Case 3: impeller surface roughness decreased by 1 order of magnitude, corresponding to polished surface finish.
Case 4: combination of impeller surface roughness, rotor weight and thrust force reduction (cases 1–3).

Figure 7 represents the resulting Pareto curves and compares them to the proof of concept and to the original optimization. All the investigated cases with design constraint relaxation yield a considerable potential for increasing the stability margin at constant seasonal performance compared to the original optimization. At the rotordynamic stability achieved by the proof of concept ($\Gamma = 0.05$), the reduced thrust force and polished impeller surface allow for an additional seasonal performance increase of 2 and 4 points, respectively, compared to the original optimization. The reduction of the rotor weight shifts the original Pareto curve toward increased stability but does not seem to additionally enhance performance. The simultaneous relaxation of all the investigated design constraints suggests an additional improvement of six points compared to the original optimization case and of 18 points compared to the proof of concept design.

Figure 8 shows the corresponding evolution of journal and thrust bearing, impeller tip, and motor diameters relative to the proof of concept design as a function of rotordynamic performance. Figure 9 indicates rotor mass and transverse inertia as well as motor length and rotor length between journals relative to the fragmented design. Compared to the proof of concept the optimizer reduces the journal diameter, thus reducing losses of both journal bearings and rotor. This trend is suggesting oversized bearings for the proof of concept design yielding too large load capacity with limited additional rotordynamic benefit. The increased impeller diameter decreases rotor speed and thus rotor windage losses. On the other hand, it leads to larger thrust forces

which need to be compensated by a larger thrust bearing yielding increased losses. Further, compared to the proof of concept, the optimizer cuts the rotor diameter of the electric motor and increases its length. Since windage losses scale with the rotor diameter at the fourth power and linearly with length this trend efficiently decreases mechanical losses. The longer rotor, however, depreciates the rotordynamic performance. This fine compromise clearly demonstrates the advantage of using an integrated approach in which the optimizer is capable of capturing the ideal trade-off, while pushing the design to its feasibility limits.

The use of lighter rotor material yields lower rotor mass and improves the rotordynamic performance as expected but does not necessarily result in increased system performance. Due to the particular rotor layout with overhung motor and impeller driving the transverse rotor inertia a lighter rotor calls for a larger distance between the journals to improve rotordynamic performance. Increased rotor length, however, requires a larger rotor diameter to avoid the flexural bending frequency from getting too close to the rotor frequency and increases the mechanical losses. Hence, a lighter rotor material does not necessarily seem to improve efficiency due to lower weight and reduced dimensions as one might expect.

The Pareto optimum curve combining the three design relaxation cases outperforms all other optimization cases as expected. A closer look at the Pareto curve and the design variables shows, however, that the combined optimization does not necessarily result in the sum of the design modifications of each individual optimization. The simultaneous relaxation of design constraints merely results in a fine tuned shift of the design variables, outlining the highly nonlinear character of the integrated system behavior.

These optimization results clearly outline the importance of integrated design approaches and demonstrate how swiftly the new methodology integrates the nonlinear behavior of the interactions between components and how it manages to successfully fine tune the very sensitive balance between contradictory objectives such as windage losses, compressor performance, and rotordynamic stability. Although the rotor layout remains the same, and the relative variation of the Pareto optimum design variables is small compared to the proof of concept design the fine-tuning of the integrated system results in a remarkable performance improvement. In addition, the novel integrated design approach is suggested to minimize the risk of unnecessary component oversizing which may deplete overall system performance.

Summary and Conclusions

The design of a direct driven radial compressor for domestic heat-pump applications on oil-free gas lubricated bearings has been formulated as a multi-objective optimization problem. Based on experimentally validated reduced order component models, the formulation enables an integrated approach as opposed to a fragmented component view, allowing to take into account for the mutual component interaction while optimizing the nonlinear system. The search for the Pareto curve has been performed by coupling the integrated system model to an evolutionary algorithm. The comparison between the resulting Pareto curve to a proof of concept that was designed using a traditional design procedure based on fragmented component view highlights the advantage of the novel integrated design procedures when designing complex, interdisciplinary systems. In this particular case, the proposed integrated design procedure allows to increase the seasonal system performance by 12 points compared to a fragmented design methodology, where each component was individually optimized. The integrated approach does not neglect the component interdependencies and allows an integrated fine-tuning of the detailed component design for minimal loss generation and maximum rotordynamic stability. It is interesting to note that the optimizer tends to compensate mechanical bearing and rotor losses by reducing the rotor speed although this is known to reduce the aerodynamic efficiency of the compressor stage. It is therefore suggested that the consideration of mutual component interactions is the key to novel and more efficient design procedures, in particular at reduced scale.

Further, the proposed approach has been applied to a design constraints based sensitivity analysis. The additional optimization runs identify impeller surface roughness and a reduction of the axial impeller thrust as key parameters for additional performance boost in small-scale turbocompressor systems. Reduced rotor weight improves rotordynamic stability but does not seem to contribute to increased seasonal performance. The combination of the investigated design constraint relaxation outperforms the original optimization run in both system performance and stability. The sensitivity analysis further reveals that the combined design constraint relaxations do not result in the sum of their individual effects. The complete system and especially the component interdependencies are highly nonlinear, and therefore the modified component interactions lead to fine-tuned modifications of the complete system design.

In addition to fine-tuning the very sensitive balance between conflicting design objectives the introduced integrated design approach prevents unnecessary component oversizing. The proposed design procedure is about to allow exiting perspectives in the domain of energy systems requiring high-speed and oil-free turbomachinery.

Acknowledgment

The author would like to thank Professor D. Favrat for the useful discussions, helpful comments, and brilliant insights.

Nomenclature

$[B]$ = system damping matrix
C = nominal bearing clearance (m)
$[C]$ = bearing damping matrix
D = diameter (m)
e = clearance (m)
E = power (W)
F = force (N)
$\mathbf{G}$ = geometry vector
$[G]$ = gyroscopic effects
H = normalized bearing groove depth
h_g = bearing groove depth (m)
I_P = polar rotor inertia (kg m^2)
I_T = transverse rotor inertia (kg m^2)
$[K]$ = system stiffness matrix
L = length (m)
m = mass flow (kg s^{-1})
$[M]$ = system inertia matrix
M_{Rot} = rotor mass (kg)
N_{Bl} = number of impeller blades
n_d = number of days
N_{Sp} = number of splitter blades
p = pressure (Pa)
$\mathbf{q}$ = system motion vector
R = radius (m)
Ra = surface roughness (m)
s = rotordynamic system eigenvalue (s^{-1})
T = temperature (°C)
w_g = groove width (m)
w_r = ridge width (m)

Greek Symbols

α = bearing groove width ratio
β = angle (bearing grooves/impeller blade) (deg)
γ = bearing groove length ratio
Γ = logarithmic decrement
η = efficiency

θ = circumferential coordinate
λ = real part of s (s^{-1})
μ = viscosity (Pa s)
Π = pressure ratio
τ = motor airgap shear stress
ω = imaginary part of s (s^{-1})
ω_{EX} = excitation speed (s^{-1})
ω_{Rot} = rotor speed (s^{-1})
Ω = whirl ratio

Subscripts

a = journal bearing a
Air = air
Ax = thrust bearing
b = journal bearing b
Back = impeller backface
g = thrust bearing groove ID
I = thrust bearing ID
Imp = impeller
In = inlet condition
Ind = inducer
J = journal bearing
Land = journal bearing land region
Mot = motor
O = thrust bearing OD
Rot = rotor
Sys = system
Tip = impeller tip
Water = water
1 = inducer
2 = impeller inlet
3 = impeller inlet blades
4 = impeller exhaust
5 = diffuser exhaust
7 = volute exhaust

Acronyms

A = air
CoG = center of gravity
HGJB = herringbone grooved journal bearing
NGT = narrow groove theory
OP = operation point
SGTB = spiral groove thrust bearing
W = water

References

[1] Schiffmann, J., 2013, "Enhanced Groove Geometry for Herringbone Grooved Journal Bearings," ASME J. Eng. Gas Turbines Power, **135**(10), p. 102501.
[2] Schiffmann, J., and Favrat, D., 2009, "Experimental Investigation of a Direct Driven Radial Compressor for Domestic Heat Pumps," Int. J. Refrig., **32**(8), pp. 1918–1928.
[3] Schiffmann, J., and Favrat, D., 2010, "Design, Experimental Investigation and Multi-Objective Optimization of a Small-Scale Radial Compressor for Heat Pump Applications," Energy, **35**(1), pp. 436–450.
[4] VDI, 1993, "Methodik Zum Entwickeln und Konstruieren Technischer Systeme und Produkte," Richtlinie-2221, Duesseldorf, Germany.
[5] Pahl, G., Beitz, W., Feldhusen, J., and Grote, K.-H., 2007, *Konstruktionslehre: Grundlagen Erfolgreicher Produkteentwicklung; Methoden und Anwendung*, Springer-Verlag, Berlin, Germany.
[6] Jarrett, J. P., Dawes, W. N., and Clarkson, P. J., 2007, "An Approach to Integrated Multi-Disciplinary Turbomachinery Design," ASME J. Turbomach., **129**(3), pp. 488–494.
[7] Schiffmann, J., and Favrat, D., 2010, "Integrated Design and Optimization of Gas Bearing Supported Rotors," ASME J. Mech. Des., **132**(5), p. 051007.
[8] Gross, W. A., Matsch, L. A., Castelli, V., Eshel, A., Vohr, J. H., and Wildmann, M., 1962, *Gas Film Lubrication*, Wiley, New York.
[9] Vohr, J. H., and Chow, C. Y., 1965, "Characteristics of Herringbone-Grooved, Gas-Lubricated Journal Bearings," ASME J. Basic Eng., **87**(3), pp. 568–578.
[10] Schiffmann, J., and Favrat, D., 2006, "Multi-Objective Optimization of Herringbone Grooved Gas Bearings Supporting a High-Speed Rotor, Taking Into Account Rarefied Gas and Real Gas Effects," ASME Paper No. ESDA2006-95086.
[11] Schiffmann, J., and Favrat, D., 2010, "The Effect of Real Gas on the Properties of Herringbone Grooved Journal Bearings," Tribol. Int., **43**(9), pp. 1602–1614.
[12] Pan, C. H. T., 1964, "Spectral Analysis of Gas Bearing Systems for Stability Studies," Mechanical Technology Inc., Latham, NY, Technical Report No. MTI 64TR58.
[13] Pan, C. H. T., and Kim, D., 2007, "Stability Characteristics of a Rigid Rotor Supported by a Gas-Lubricated Spiral-Groove Conical Bearing," ASME J. Tribol., **129**(2), pp. 375–383.
[14] Cunningham, R. E., Fleming, D. P., and Anderson, W. J., 1971, "Experimental Load Capacity and Power Loss of Herringbone Grooved Gas Lubricated Journal Bearings," J. Lubr. Technol., **93**(3), pp. 415–422.
[15] Mack, M., 1967, "Luftreibungsverluste Bei Elektrischen Maschinen Kleiner Baugrösse," Ph.D. thesis, Universität Stuttgart (FH), Stuttgart, Germany.
[16] Keskin, A., and Bestle, D., 2006, "Application of Multi-Objective Optimization to Axial Compressor Preliminary Design," Aerosp. Sci. Technol., **10**(7), pp. 581–589.
[17] Galvas, M. R., 1973, "Fortran Program for Predicting Off-Design Performance of Centrifugal Compressors," NASA Lewis Research Center, Cleveland, OH, Technical Report No. TN D-7487.
[18] Senoo, Y., and Kinoshita, Y., 1977, "Influence of Inlet Flow Conditions and Geometries of Centrifugal Vaneless Diffuser on Critical Flow Angle for Reverse Flow," ASME J. Fluids Eng., **99**(1), pp. 98–103.
[19] Miller, T. J. E., 1993, *Switched Reluctance Motors and Their Control*, Magna Physics Publishing, Oxford Science Publications, Oxford, UK.
[20] Schiffmann, J., Favrat, D., and Molyneaux, A., 2004, "Compresseur Radial Pour Pompe à Chaleur Biétagée, Phase 2," Swiss Federal Office for Energy, Bern, Switzerland, Technical Report OFEN, ENET-Nr. 100133.
[21] Binder, A., Schneider, T., and Klohr, M., 2006, "Fixation of Buried and Surface-Mounted Magnets in High-Speed Permanent-Magnet Synchronous Machines," IEEE Trans. Ind. Appl., **42**(4), pp. 1031–1037.
[22] Schiffmann, J., 2008, "Integrated Design, Optimization and Experimental Investigation of a Direct Driven Turbocompressor for Domestic Heat Pumps," Ph.D. thesis, Ecole Polytechnique Federale de Lausanne, Lausanne, Switzerland.
[23] Molyneaux, A., Leyland, G. B., and Favrat, D., 2010, "Environomic Multi-Objective Optimization of a District Heating Network Considering Centralized and Decentralized Heat Pumps," Energy, **35**(2), pp. 751–758.
[24] Schiffmann, J., and Spakovszky, Z. S., 2013, "Foil Bearing Design Guidelines for Improved Stability," ASME J. Tribol., **135**(1), p. 011103.
[25] Leyland, G. B., 2002, "Multi-Objective Optimization Applied to Industrial Energy Problems," Ph.D. thesis, Ecole Polytechnique Federale de Lausanne, Lausanne, Switzerland.
[26] Casey, M. V., and Marti, F., 1986, "Centrifugal Compressors—Performance at Design and Off-Design," Institute of Refrigeration at the Institute of Marine Engineers, London, UK.
[27] Balje, O. E., 1981, *Turbomachines, A Guide to Design, Selection and Theory*, Wiley, New York.